

# Retinal cell imaging in myopic chickens using adaptive optics multiphoton microscopy

Juan M. Bueno,<sup>1,\*</sup> Raquel Palacios, Anastasia Giakoumaki,<sup>1</sup> Emilio J. Gualda,<sup>1</sup>  
Frank Schaeffel,<sup>2</sup> and Pablo Artal<sup>1</sup>

<sup>1</sup>Laboratorio de Óptica, Instituto Universitario de Investigación en Óptica y Nanofísica, Universidad de Murcia, Campus de Espinardo (Ed.34), 30100 Murcia, Spain

<sup>2</sup>Section of Neurobiology of the Eye, Ophthalmic Research Institute, Calwerstrasse 7/1, 72076 Tuebingen, Germany  
\*bueno@um.es

**Abstract:** Abnormal eye growth induced by visual deprivation can modify the structure and density of the retinal cells. We have used an adaptive optics multiphoton microscope to image photoreceptors (PRs) and ganglion cells (GCs) at different retinal locations in unstained retinas of chicken eyes with about 10D of myopia and their normal-sighted fellow eyes. In all samples, the local averaged inter-PR distance increased with eccentricity. No significant differences in PR density were found between control and myopic eyes. GC density declined in myopic eyes compared to control eyes and the inter-cell distance increased. In normal eyes, the size of the GC cell bodies increased approximately two-fold between the area centralis and the peripheral retina. In myopic eyes, this trend was preserved but the GC bodies were larger at each retinal location, compared to control eyes. Obviously, GC morphology is changing when the retinal area is enlarged in myopic eyes.

©2014 Optical Society of America

**OCIS codes:** (170.3880) Medical and biological imaging; (180.4315) Nonlinear microscopy; (110.1080) Active or adaptive optics; (170.4470) Ophthalmology

## References and links

1. J. Wallman, J. Turkel, and J. Trachtman, "Extreme myopia produced by modest change in early visual experience," *Science* **201**(4362), 1249–1251 (1978).
2. F. Schaeffel, A. Glasser, and H. C. Howland, "Accommodation, refractive error and eye growth in chickens," *Vision Res.* **28**(5), 639–657 (1988).
3. C. F. Wildsoet and J. D. Pettigrew, "Experimental myopia and anomalous eye growth-patterns unaffected by optic-nerve section in chickens: Evidence for local-control of eye growth," *Clin. Vis. Sci.* **3**, 99–107 (1988).
4. J. G. Sivak, D. L. Barrie, and J. A. Weerheim, "Bilateral experimental myopia in chicks," *Optom. Vis. Sci.* **66**(12), 854–858 (1989).
5. D. Troilo and J. Wallman, "The regulation of eye growth and refractive state: an experimental study of emmetropization," *Vision Res.* **31**(7-8), 1237–1250 (1991).
6. Y. F. Shih, M. E. Fitzgerald, T. T. Norton, P. D. Gamlin, W. Hodos, and A. Reiner, "Reduction in choroidal blood flow occurs in chicks wearing goggles that induce eye growth toward myopia," *Curr. Eye Res.* **12**(3), 219–227 (1993).
7. J. Wallman, C. Wildsoet, A. Xu, M. D. Gottlieb, D. L. Nickla, L. Marran, W. Krebs, and A. M. Christensen, "Moving the retina: choroidal modulation of refractive state," *Vision Res.* **35**(1), 37–50 (1995).
8. H. Liang, D. P. Crewther, S. G. Crewther, and A. M. Barila, "A role for photoreceptor outer segments in the induction of deprivation myopia," *Vision Res.* **35**(9), 1217–1225 (1995).
9. X. Zhu, T. Lin, R. A. Stone, and A. M. Laties, "Sex differences in chick eye growth and experimental myopia," *Exp. Eye Res.* **61**(2), 173–179 (1995).
10. J. R. Phillips, M. Khalaj, and N. A. McBrien, "Induced myopia associated with increased scleral creep in chick and tree shrew eyes," *Invest. Ophthalmol. Vis. Sci.* **41**(8), 2028–2034 (2000).
11. S. Y. Kim, N. Ondhia, D. Vidgen, L. Malaval, M. Ringuette, and V. I. Kalnins, "Spatiotemporal distribution of SPARC/osteonectin in developing and mature chicken retina," *Exp. Eye Res.* **65**(5), 681–689 (1997).
12. Y. A. Kram, S. Mantey, and J. C. Corbo, "Avian cone photoreceptors tile the retina as five independent, self-organizing mosaics," *PLoS ONE* **5**(2), e8992 (2010).

13. C. J. Wolsley, K. J. Saunders, G. Silvestri, and R. S. Anderson, "Investigation of changes in the myopic retina using multifocal electroretinograms, optical coherence tomography and peripheral resolution acuity," *Vision Res.* **48**(14), 1554–1561 (2008).
14. M. L. Kislak, K. Bunghardt, J. J. Hunter, E. L. Irving, and M. C. W. Campbell, "Longitudinal in vivo imaging of cones in the alert chicken," *Optom. Vis. Sci.* **89**(5), 644–651 (2012).
15. K. Headington, S. S. Choi, D. Nickla, and N. Doble, "Single cell imaging of the chick retina with adaptive optics," *Curr. Eye Res.* **36**(10), 947–957 (2011).
16. J. M. Bueno, A. Giakoumaki, E. J. Gualda, F. Schaeffel, and P. Artal, "Analysis of the chicken retina with an adaptive optics multiphoton microscope," *Biomed. Opt. Express* **2**(6), 1637–1648 (2011).
17. W. Denk, J. H. Strickler, and W. W. Webb, "Two-photon laser scanning fluorescence microscopy," *Science* **248**(4951), 73–76 (1990).
18. Y. Imanishi, M. L. Batten, D. W. Piston, W. Baehr, and K. Palczewski, "Noninvasive two-photon imaging reveals retinyl ester storage structures in the eye," *J. Cell Biol.* **164**(3), 373–383 (2004).
19. Y. Imanishi, K. H. Lodowski, and Y. Koutalos, "Two-photon microscopy: Shedding light on the chemistry of vision," *Biochemistry* **46**(34), 9674–9684 (2007).
20. B. G. Wang, A. Eitner, J. Lindenau, and K. J. Halhuber, "High-resolution two-photon excitation microscopy of ocular tissues in porcine eye," *Lasers Surg. Med.* **40**(4), 247–256 (2008).
21. J. J. Mancuso, A. M. Larson, T. G. Wensel, and P. Saggau, "Multiphoton adaptation of a commercial low-cost confocal microscope for live tissue imaging," *J. Biomed. Opt.* **14**(3), 034048 (2009).
22. R.-W. Lu, Y.-C. Li, T. Ye, C. Strang, K. Keyser, C. A. Curcio, and X.-C. Yao, "Two-photon excited autofluorescence imaging of freshly isolated frog retinas," *Biomed. Opt. Express* **2**(6), 1494–1503 (2011).
23. E. J. Gualda, J. M. Bueno, and P. Artal, "Wavefront optimized non-linear microscopy of ex vivo human retinas," *J. Biomed. Opt.* **15**(2), 026007 (2010).
24. M. Han, A. Bindewald-Wittich, F. G. Holz, G. Giese, M. H. Niemz, S. Snyder, H. Sun, J. Y. Yu, M. Agopov, O. La Schiazza, and J. F. Bille, "Two-photon excited autofluorescence imaging of human retinal pigment epithelial cells," *J. Biomed. Opt.* **11**(1), 010501 (2006).
25. M. Han, G. Giese, S. Schmitz-Valckenberg, A. Bindewald-Wittich, F. G. Holz, J. Y. Yu, J. F. Bille, and M. H. Niemz, "Age-related structural abnormalities in the human retina-choroid complex revealed by two-photon excited autofluorescence imaging," *J. Biomed. Opt.* **12**(2), 024012 (2007).
26. J. F. Bille, M. Agopov, C. Alvarez-Diez, M. Han, N. Korablion, U. Von Pape, M. Olivier La Schiazza, M. Schwingel, H. Zhang, and F. Muller, "Compact adaptive optics system for multiphoton fundus imaging," *J. Mod. Opt.* **55**(4–5), 749–758 (2008).
27. J. M. Bueno, E. J. Gualda, and P. Artal, "Adaptive optics multiphoton microscopy to study ex vivo ocular tissues," *J. Biomed. Opt.* **15**(6), 066004 (2010).
28. J. J. Hunter, B. Masella, A. Dubra, R. Sharma, L. Yin, W. H. Merigan, G. Palczewska, K. Palczewski, and D. R. Williams, "Images of photoreceptors in living primate eyes using adaptive optics two-photon ophthalmoscopy," *Biomed. Opt. Express* **2**(1), 139–148 (2011).
29. D. Troilo, M. Xiong, J. C. Crowley, and B. L. Finlay, "Factors controlling the dendritic arborization of retinal ganglion cells," *Vis. Neurosci.* **13**(4), 721–733 (1996).
30. F. Schaeffel and H. C. Howland, "Visual optics in normal and ametropic chickens," *Clin. Vis. Sci.* **3**, 83–89 (1988).
31. J. D. Pettigrew, A. Bhagwandin, M. Haagenzen, and P. R. Manger, "Visual acuity and heterogeneities of retinal ganglion cell densities and the tapetum lucidum of the African elephant (*Loxodonta africana*)," *Brain Behav. Evol.* **75**(4), 251–261 (2010).
32. F. Schaeffel and H. C. Howland, "Properties of the feedback loops controlling eye growth and refractive state in the chicken," *Vision Res.* **31**(4), 717–734 (1991).
33. A. Seidemann and F. Schaeffel, "Effects of longitudinal chromatic aberration on accommodation and emmetropization," *Vision Res.* **42**(21), 2409–2417 (2002).
34. M. Bartmann and F. Schaeffel, "A simple mechanism for emmetropization without cues from accommodation or colour," *Vision Res.* **34**(7), 873–876 (1994).
35. N. S. Hart, T. J. Lisney, and S. P. Collin, "Cone photoreceptor oil droplet pigmentation is affected by ambient light intensity," *J. Exp. Biol.* **209**(23), 4776–4787 (2006).
36. Y. Chui, M. Yap, and H. Chan, "The retinal ganglion cell density and nerve fiber layer thickness in the human myopic eye," *Invest. Ophthalmol. Vis. Sci.* **43**, 183 E-Abstract (2002).
37. H. E. Grossniklaus and W. R. Green, "Pathologic findings in pathologic myopia," *Retina* **12**(2), 127–133 (1992).
38. Y. Kitaguchi, K. Bessho, T. Yamaguchi, N. Nakazawa, T. Mihashi, and T. Fujikado, "In vivo measurements of cone photoreceptor spacing in myopic eyes from images obtained by an adaptive optics fundus camera," *Jpn. J. Ophthalmol.* **51**(6), 456–461 (2007).
39. T. Y. P. Chui, H.-X. Song, and S. A. Burns, "Individual variations in human cone photoreceptor packing density: variations with refractive error," *Invest. Ophthalmol. Vis. Sci.* **49**(10), 4679–4687 (2008).
40. K. Y. Li, P. Tiruveedhula, and A. Roorda, "Intersubject variability of foveal cone photoreceptor density in relation to eye length," *Invest. Ophthalmol. Vis. Sci.* **51**(12), 6858–6867 (2010).
41. V. B. Morris, "Symmetry in a receptor mosaic demonstrated in the chick from the frequencies, spacing and arrangement of the types of retinal receptor," *J. Comp. Neurol.* **140**(3), 359–397 (1970).

42. J. K. Bowmaker and A. Knowles, "The visual pigments and oil droplets of the chicken retina," *Vision Res.* **17**(7), 755–764 (1977).
  43. R. Over and D. Moore, "Spatial acuity of the chicken," *Brain Res.* **211**(2), 424–426 (1981).
  44. H. M. Johnson, "Visual pattern-discrimination in the vertebrate: II. Comparative visual acuity in the dog, the monkey and the chick," *J. Anim. Behav.* **4**(5), 340–361 (1914).
  45. L. R. DeMello, T. M. Foster, and W. Temple, "Discriminative performance of the domestic hen in a visual acuity task," *J. Exp. Anal. Behav.* **58**(1), 147–157 (1992).
  46. K. L. Schmid and C. F. Wildsoet, "Assessment of visual acuity and contrast sensitivity in the chick using an optokinetic nystagmus paradigm," *Vision Res.* **38**(17), 2629–2634 (1998).
  47. E. Diedrich and F. Schaeffel, "Spatial resolution, contrast sensitivity, and sensitivity to defocus of chicken retinal ganglion cells in vitro," *Vis. Neurosci.* **26**(5-6), 467–476 (2009).
  48. N. J. Coletta and T. Watson, "Effect of myopia on visual acuity measured with laser interference fringes," *Vision Res.* **46**(5), 636–651 (2006).
  49. T. Y. Chui, M. K. Yap, H. H. Chan, and L. N. Thibos, "Retinal stretching limits peripheral visual acuity in myopia," *Vision Res.* **45**(5), 593–605 (2005).
- 

## 1. Introduction

Chickens have been extensively used as animal model in emmetropization and myopia studies. It is well established that deprivation by placing diffusers in front of their eyes alters the normal ocular growth pattern within hours, generating excessive axial elongation and subsequent myopia [1–5]. The growth of the posterior globe is controlled largely by the retina which can inhibit or stimulate scleral growth, depending on the sign of the defocus imposed on the retinal image. As a result, the best match between the focal plane and the photoreceptor (PR) plane is achieved during development [1]. When excessive growth is induced by negative lenses or diffusers, choroidal blood flow is reduced [6], choroidal thinning occurs [7], and the cone inner segments thicken and rod outer segments elongate [8]. The anterior chamber depth enlarges [9] and the scleral creep rate increases, at least in mammalian myopia models [10]. The chicken retinal structures have been imaged with fluorescence [11] and brightfield microscopy [12], OCT [13] and more recently with confocal scanning laser ophthalmoscopy [14], adaptive optics (AO) fundus imaging [15], and AO multiphoton microscopy [16].

Two-photon excitation fluorescence (TPEF) [17] has been reported to be a multiphoton tool suitable for imaging biological specimens. Since Imanishi and colleagues reported that both the retinal pigment epithelium (RPE) [18] and the PR outer segments [19] of the mouse retina provided TPEF signal, different authors have explored the visualization and distribution of retinal cells in animal models [20–22] and humans [23–26]. In particular, the combination of AO and multiphoton microscopy provided improved images of every retinal layer in non-stained human and chicken retinas [16,23,27]. AO multiphoton ophthalmoscopy also provided images of PRs in living primate eyes [28].

Although chicken retinal cells have recently been imaged in vivo [25,26], there are few data on the effects of induced myopia on retinal cell spacing, distribution and density in chickens, except for a histological study on the spacing and arborization of retinal beta ganglion cells [29]. Moreover, PR densities have not been mapped out. Non-linear imaging techniques are minimally invasive and provide intrinsic axial resolution, allowing imaging of the different retinal structures without staining procedures. In this sense, the aim of this work has been to use AO-TPEF microscopy in retinas of myopic chickens to study the spacing, appearance and distribution of retinal cells to be compared with normal chicken eyes.

## 2. Methods

### 2.1. Adaptive optics multiphoton microscopy

Multiphoton imaging was performed using a research custom-built scanning microscope, combining a mode-locked Ti:Sapphire laser (760 nm), a modified inverted microscope and a photon-counting unit detection (Fig. 1). Further details can be found in [16,27]. The setup also includes an AO module composed of a Hartmann-Shack wavefront sensor and a deformable

mirror, used to compensate for the laser beam and microscope optics aberrations in closed-loop. A DC-motor controlled the location of imaged plane within the sample along the Z direction. A non-immersion long-working distance microscope objective was used (20x, NA = 0.5). TPEF signal from the sample was collected in the backscattered direction through the same objective. A spectral filter was placed in front of the detection unit (PMT) to select this TPEF signal. All TPEF images shown along this paper were recorded with the AO module in operation. At the specimen plane, and depending on the analyzed sample, the laser intensity ranged between 2 and 20 mW/cm<sup>2</sup>.

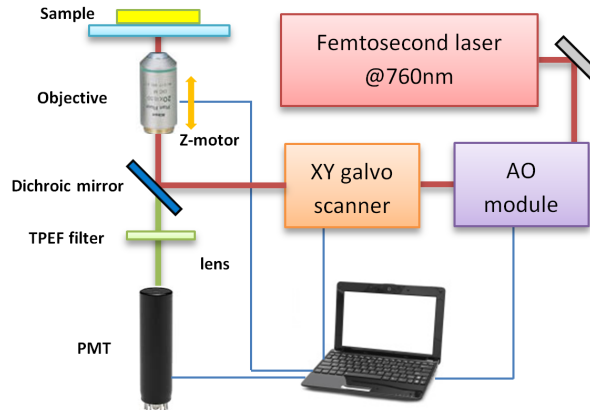


Fig. 1. Schematic diagram of the AO multiphoton microscope. PMT, photomultiplier.

Image acquisition was carried out by means of custom-written LabView<sup>TM</sup> software. TPEF microscopy images were recorded at a rate of 1 image per second (0.82 microns/pixel) at different eccentricities along the retinal depth (in steps of 3 microns). Having into account the used wavelength and the microscope objective specifications, the theoretical lateral and axial resolution values for a multiphoton configuration are respectively 0.52 and 2.13 microns.

Although TPEF signal clearly visualizes most retinal layers from the nerve fiber layer to the PR outer segment [16], in the present work we are only interested in evaluating the spatial distribution of PRs and GCs in both control and myopic retinas. At each retinal depth-location six individual frames were acquired and averaged to get the final image. Image processing was performed using both MatLab<sup>TM</sup> and the public domain image processing software ImageJ.

For each image the density of PRs was manually computed by the operator [16]. To calculate the density (and area) of GCs, each image was first processed using different filters to improve the visibility of the GCs (Fig. 2(a)). This included brightness-contrast adjust, background subtraction and median filtering. Then an image contrast threshold and a binary process was also applied (Fig. 2(b)). Watershed segmentation was employed to automatically separate individual GCs (Fig. 2(c)). Cells located on the edges of the image were not taken into account. Sometimes, as a result of the automatic segmentation procedure, small and irregular particles are generated as artefacts. These were also excluded from the final computation. Finally the quantity of GCs within the image and the area for each individual GC were calculated (Fig. 2(d)).

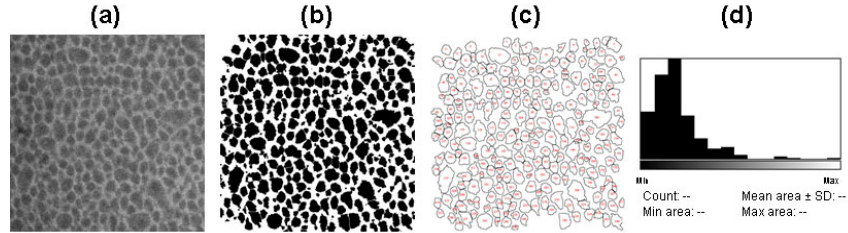


Fig. 2. Example of the procedure steps. (a) TPEF image of GCs; (b) image after different filtering, thresholding and binarization; (c) watershed segmentation; (d) final histogram for GC counting and area computation.

The area centralis of the chicken retina has been reported to be the location with maximum cell density [15,16]. For each retina it was located in a previous operation by using a bright-field (linear) microscope. With this technique, only the PR oil droplets are clearly visible [16]. Two different observers (co-authors) independently chose the location that was always similar for both. This was set as the origin of the eccentricity scale.

To determine the retinal eccentricities from the linear distances on the retinal surface, the values of posterior nodal distance (PND) and radius of the ocular globes of schematic chicken eye models (both emmetropic and myopic) were used [30].

Moreover, the visual spatial resolution (VR, in cycles/deg) of the chicken retina for different eccentricities was calculated as [31]:

$$VR = \frac{\pi}{180} \cdot \frac{PND}{2 \cdot D_{GC}}, \quad (1)$$

with  $D_{GC}$  being the averaged GC inter-distance directly computed from the Fourier power spectrum of the GC images [16].

## 2.2. Samples

Five male white leghorn chicks were obtained from a local hatchery in Kilchberg, Germany, and raised in groups under a 12-hr light/12-hr dark cycle in the animal facilities of the Institute for Ophthalmic Research (Section of Neurobiology of the Eye) in Tuebingen, Germany. Food and water were freely available. For the development of myopia, chickens wore diffusers over one eye for 7 days according to a well-established procedure [32]. The fellow eyes had normal visual experience and were used as controls for comparison. After diffuser removal, ocular refraction was measured using automated infrared photorefractometry [33]. After one week of diffuser wearing three out of five eyes developed myopia of  $-10.4 \pm 2.9$  D on average. The two eyes which became scarcely myopic were excluded from the study. As typically found, fellow control eyes exposed to normal vision remained near-emmetropic ( $1.3 \pm 1.6$  D). The animals (4 week-old) were sacrificed with an overdose of ethyl ether anesthesia (see further details on [34]) and the ocular globes were immediately excised. After cutting the ocular globe along the horizontal plane behind the scleral ossicles, the vitreous was extracted and the retina detached from the fundus. The retina (without the RPE) was fixed overnight in a moist chamber with paraformaldehyde solution (4%, in 0.1M phosphate buffer). The retinal tissue was flat-mounted on a microscope slide and covered with a 130- $\mu$ m thick cover slip. None of the samples was stained. A total of eight retinas (3 myopic, 5 control) were involved in the present study. Control eyes were the same as those used in [16]. Experiments were conducted in accordance with the statement for the use of Animals in Ophthalmic and Vision Research and approved by the University of Tuebingen Commission for Animal Welfare.

### 3. Results

#### 3.1. Visualization and analysis of the PR mosaic

Despite the transparency of the retinal tissues in the visible part of the spectrum, multiphoton microscopy provides images with sufficient contrast across the entire retina. As an example, Fig. 3 shows images of the PR mosaic in a control and an after deprivation myopia eye. TPEF signals clearly denote individual cells in both images. Since the samples were not stained, this signal corresponds to endogenous fluorescence. At the PR layer the signal comes mainly from the oil droplets, heavily pigmented spherical organelles located between the inner and the outer segment [35].

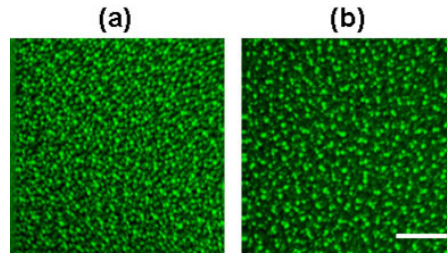


Fig. 3. TPEF images of PR layer for control (a) and myopic (b) chicken retinas at the same retinal eccentricity. Sets of PR images for various retinal eccentricities previously reported by these authors can be seen in [16]. Scale bar: 50 microns.

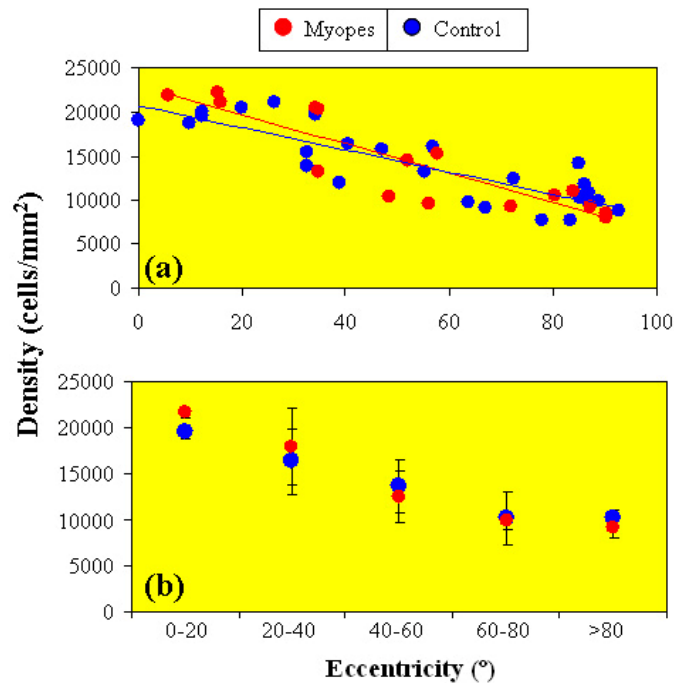


Fig. 4. (a) Decrease in PR density (cells/mm<sup>2</sup>) with retinal eccentricity for myopic (red symbols) and control (blue symbols) eyes. Linear regressions fitted to the data demonstrate a significant decrease in PR density with retinal eccentricity. (b) Averaged PR density values as a function of the retinal eccentricity grouped in intervals of 20 degrees.

In order to evaluate the spatial distribution of PR in both control and myopic eyes TPEF images of the corresponding layer were acquired at different retinal eccentricities. Figure 4(a) shows the density of PRs for all specimens as a function of the retinal eccentricity in both

myopic (red) and control (blue) eyes. Blue and red lines are the corresponding best linear fits which showed a significant decrease with eccentricity ( $R^2 = 0.79$ ,  $p < 0.0001$  and  $R^2 = 0.74$ ,  $p < 0.001$  respectively). A paired t-test showed not significant differences between both sets of data. For completeness, the changes in PR density with retinal eccentricity grouped in intervals of 20 degrees are shown in Fig. 4(b). At the central retina the PR density for these particular samples was about 20600 cells/mm<sup>2</sup>. These values decreased to approximately one half at the peripheral regions of the retina.

To further explore this spatial distribution of PRs, for each TPEF image the local average PR inter-distance was computed from the Fourier power spectrum [16]. For both myopic and control samples the increase in PR inter-distance as a function of retinal eccentricity is depicted in Fig. 5(a) and the relationship between this PR inter-distance and the density of PRs in Fig. 5(b). For both plots significant linear correlations were found:  $R^2 = 0.40$ ,  $p = 0.008$  and  $R^2 = 0.36$ ,  $p = 0.001$  for myopic and control eyes respectively in Fig. 5(a), and  $R^2 = 0.61$ ,  $p = 0.003$  and  $R^2 = 0.56$ ,  $p < 0.001$  for results in Fig. 5(b). As also shown in Fig. 4, distributions for myopic and control eyes did not differ significantly.

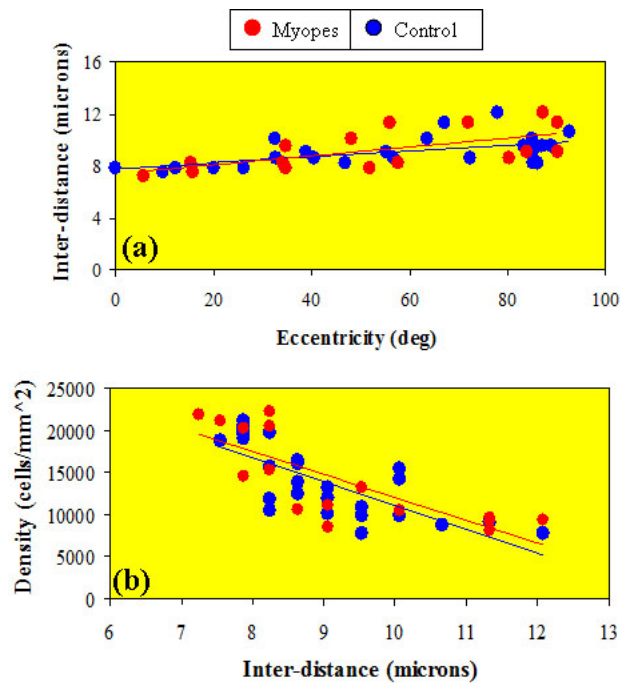


Fig. 5. (a) Increase in PR inter-distance with retinal eccentricity. (b) PR inter-distance (microns) versus PR density (cells/mm<sup>2</sup>). Myopic and control eyes are represented by red and blue symbols respectively. Linear regressions fitted to the data demonstrate a significant increase in (a) and a significant decrease in (b) for both sets of retinas.

### 3.2. Visualization and analysis of the GC layer

TPEF images of the GC layer in control and myopic eyes for two different retinal eccentricities are shown in Fig. 6. Whereas the cell nucleus remains dark, the borders (cytoplasm) provides a high non-linear signal, allowing readily distinguishing individual cells at every retinal location.

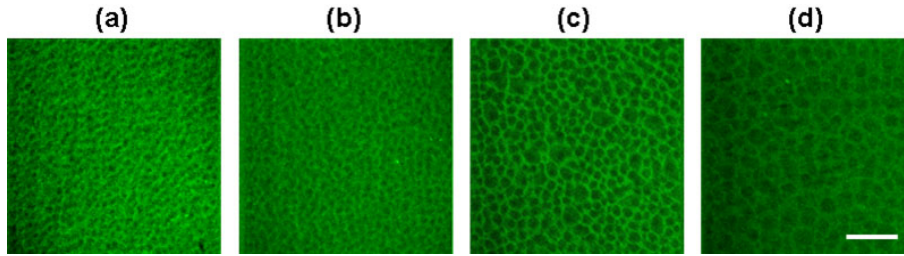


Fig. 6. TPEF images of GCs for control (a, c) and myopic (b, d) eyes. Images correspond to different retinal eccentricities,  $\sim 15^\circ$  (a, b) and  $\sim 85^\circ$  (c, d). Scale bar: 50 microns.

The density of GCs was also computed for different retinal locations. Figure 7 presents the results. A significant decrease with retinal eccentricity was also found for both myopic ( $R^2 = 0.64$ ,  $p < 0.017$ ) and control ( $R^2 = 0.86$ ,  $p < 0.0001$ ) retinas. Overall GC density for eyes exhibiting deprivation myopia was 13% lower than that of controls ones, although this difference did not achieve significance.

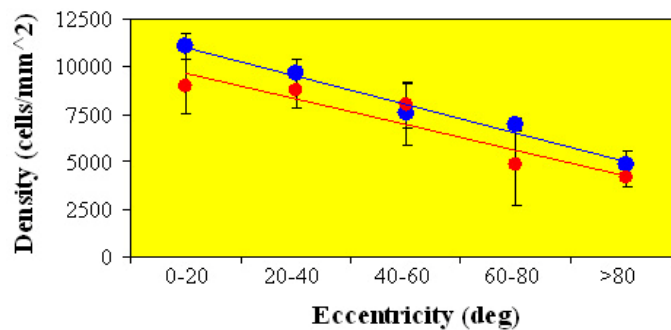


Fig. 7. Change in GC density (cells/mm<sup>2</sup>) as a function of the retinal eccentricity grouped in intervals of 20 degrees, for myopic (red symbols) and control (blue symbols) retinas.

The changes in GC area with retinal location are depicted in Fig. 8. A significant increase in GC body size with retina eccentricity was observed for myopic ( $R^2 = 0.42$ ,  $p = 0.058$ ) and control retinas ( $R^2 = 0.49$ ,  $p = 0.003$ ). It is interesting to note that the size of the GCs increased approximately two-fold when comparing the area centralis and the peripheral retina. For each retinal location, the GC size in after deprivation retinas was larger than in control ones (83% on average). Moreover, this difference was statistically significant ( $p = 0.01$ , paired t-test).

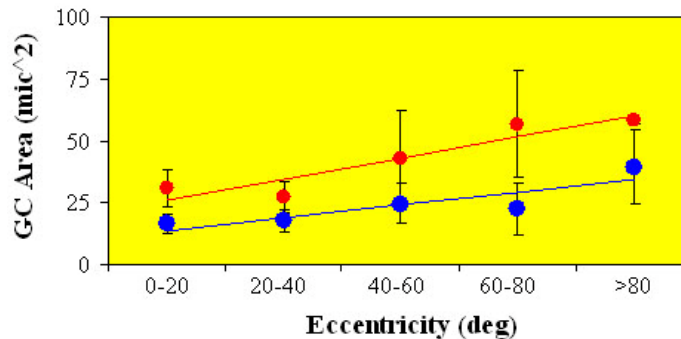


Fig. 8. Averaged GC area values (microns<sup>2</sup>) for different retinal eccentricities. Red symbols, myopic; blue symbols, control. Lines correspond to the best linear fits.

For completeness, Fig. 9 shows the corresponding values of GC inter-distance (parameter  $D_{GC}$ ). As expected, for both types of retinas, the increase with eccentricity was significant. Moreover, for each retinal location  $D_{GC}$  was larger in myopic eyes (24% on average), and this difference was statistically significant ( $p = 0.005$ , paired t-test).

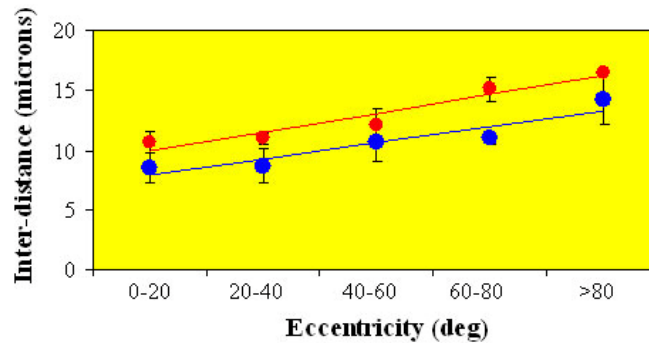


Fig. 9. Significant linear increase of GC inter-distance (microns) with retinal eccentricity. Myopic eyes (red dots):  $R = 0.77$ ,  $p = 0.015$ ; control eyes (blue dots):  $R = 0.80$ ,  $p = 0.0001$ .

From each TPEF image of GCs, the VR was computed as explained in Eq. (1). As expected, VR decreased towards the retinal periphery (as depicted in Fig. 10) for control and (optically corrected) myopic eyes. For most retinal locations VR appeared higher in control retinas (14% on average, 20% at the area centralis) but this difference did not achieve significance either.

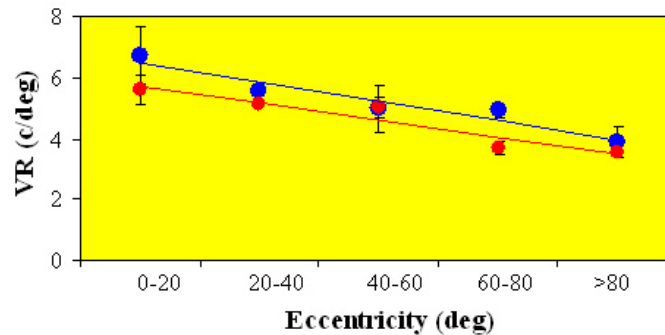


Fig. 10. Values of calculated GC visual resolution (c/deg) in the chick retina as a function of retinal eccentricity computed using Eq. (1). Labels are the same as in previous figures.

#### 4. Discussion

AO multiphoton microscopy has been used to image retinal layers containing PRs and GCs in both control and myopic chicken eyes. Individual cells are clearly distinguished in all specimens. Parameters such as cell density and inter-distance have been analyzed for different eccentricities in order to provide additional information on cellular arrangement. Although retinal cells have been imaged with this microscopy technique [20–22,24–27], to our knowledge this is the first time that TPEF images have been used to compare densities and spacial distributions between myopic and emmetropic eyes.

Results herein have shown that PR density decreased with retinal eccentricity in myopic and control eyes. However, no difference in PR density was detected in myopic eyes compared to normal fellow eyes. Cone inter-distance was significantly related to density in both sets of eyes. GC density declined by 13% when myopia was induced (which did not achieve significance). This agrees with the increase in surface of the ocular globe of about 18% for a 10-D myopic chicken eye. Moreover, the averaged spacing among GCs increased

by 24%. This latter finding is very similar to the result reported by Troilo et al. ([29], their Fig. 7): retinal tissue is simply stretched during myopia development but no further GCs are added.

Furthermore, it was found that GC densities declined from the center to the periphery by about 60%, and cell bodies became larger by a factor of about 2. This pattern was preserved all over the visual field and it was not affected by retinal stretching during myopia development (see Fig. 8). The lack of local changes of the GC parameters suggests a linear expansion of the chicken globe during myopia development. In fact, a scaled expansion of the posterior globe during development of deprivation myopia was already described by Wallman and associates [1] based on tracings of the external shape of the globe.

There is a special interest in exploring the changes produced in myopic eyes and the reasons for those changes. There is a lack of studies comparing retinal cell distributions between myopic and emmetropic eyes, although Troilo and associates [29] reported some results on form deprivation chickens and GC distribution. They found a 20-30% increase in GC density in myopic chickens. Results in human eyes (using a custom-designed retinal acuity perimeter) reported that the GC density significantly reduced with increasing myopia in both central and peripheral retina [36]. We also observed this in chickens although the decrease was not statistically significant.

A histological study of human retinas reported that the PR density was lower in eyes with pathological myopia than in eyes with emmetropia [37]. The implementation of AO devices into confocal ophthalmoscopes and fundus cameras has provided a tool to explore differences in cone density in normal and myopic living human eyes. Despite that different authors have explored this question, they do not fully agree on each other. Kitaguchi and colleagues reported that at 2 deg from the fovea the average cone spacing in moderate- to high-myopia groups was significantly larger than in the normal and low-myopia groups [38]. Chui et al. imaged cones at different retinal locations in emmetropic and myopic human eyes. They reported that cone density was significantly lower in myopic eyes, although at a given location, there was considerable individual variation [39]. This intersubject variability was also reported by Li and collaborators [40]. Myopic eyes were found generally to have higher angular density near the foveal center. However at 1 deg this was nullified by retinal expansion, what means that angular densities across all eyes were similar.

The PR counting performed here included all types of PRs (i.e. single and double). For all retinas the highest density was found at the area centralis:  $19528 \pm 701$  and  $21648 \pm 563$  cells/mm<sup>2</sup> for control and for myopic retinas respectively. These values were similar to those reported by Headington et al. [15] (20980-25148 cells/mm<sup>2</sup>) but higher than those found by Moris [41] (16576 cells/mm<sup>2</sup>) and Bowmaker and associates [42] (10021 cells/mm<sup>2</sup>). Our mean PR density at 40 deg (~16500 and ~18000 cells/mm<sup>2</sup> in control and myopic eyes) was similar to that reported by Kram and associates [12] at the mid-peripheral retina in four quadrants for all type of single cones (17585 cones/mm<sup>2</sup>) but much lower than Headington et al.'s values [15] (21714 and 26105 cells/mm<sup>2</sup>). At the peripheral retina we found a mean of ~10000 cells/mm<sup>2</sup>, a number somewhat lower than 13760 cells/mm<sup>2</sup> previously reported by Morris [41].

In the counting procedure here reported all the PRs took part. A step forward would be trying to differentiate single from double PRs in non-stained chicken retinas. Bright-field microscopy has shown that both types of PRs provide different spectral sensitivity. Since a unique wavelength is used in multiphoton microscopy, spectral properties might be missed and it would be hard to separate both types of cells. More complex imaging procedures (such as Voronoi analysis [12,14,15]) might be very helpful, although this is out of the scope of this work.

The visualization of the GC in the TPEF images also allowed us to compute the anatomically-based VR. This parameter decreased towards the periphery and was higher in emmetropic eyes than in myopic eyes (although not significantly). VR and spatial acuity have

been previously measured in chickens using different methods. Earlier studies reported VR values ranging from 1.5 c/deg for 1- to 25-day-old chicks [43] to about 7 c/deg for 6-month old birds [44]. Later Demello and collaborators [45] reported 4-6 c/deg in adult chickens, and Schmid and Wildsoet [46] measured 7.7-8.6 c/deg in 8-day old chickens. More recently Diedrich and Schaeffel found 4-5 c/deg in 6 day-old chickens [47]. In this work averaged values of 6.7 and 5.6 c/deg were obtained at the area centralis for emmetropic and myopic eyes respectively. However data for different retinal eccentricities or comparisons between control and after form deprivation eyes have not been found in the literature by these authors.

Different studies analyzed the VR in humans for different retinal eccentricities and refractive states. Colleta and Watson [48] reported a decreased VR with increasing myopia at three retinal locations. This implies that retinal cells in highly myopic eyes are more widely spaced than in normal. Chui et al. [49] found a linear decrease with magnitude of refractive error in VR at every retinal location. This was attributed to changes in cell spacing due to the retinal stretching. This effect was noticeable at the peripheral field of myopic eyes, but was only occasionally detectable in the fovea. Although humans and chickens might not be directly comparable, an increase in GC spacing with myopia and the corresponding decrease in VR was also found in this work.

Results on the change in density and size of GCs here reported are consistent with the stretching of the retina in form deprivation myopic chicken eyes. However, at this point a question arises: Why was no reduction in PR density observed in our myopic chicken eyes? A first hypothesis might be based on the fact that during myopia development new PRs are added from the periphery but there is no evidence for this claim (A. J. Fischer, personal communication 2013). A second possibility is that the transversal size of some PRs is smaller than the resolution limit of our microscope. This would lead to an underestimation of the PR density since sets of PRs might have not been into account for density calculation. Third, deprivation myopia has been reported to produce a significant displacement of the PR tips [8]. It could be also hypothesized that this “movement” might displace the oil droplets of a number of PRs to planes above or below the imaged plane. The corresponding PRs would be missed in the recorded image and the actual density would be above the computed one. If PR density keeps constant but GC spacing increases, this would indicate a higher convergence ratio for the PRs in the myopic eye.

In conclusion, this study shows the power of AO multiphoton microscopy to differentiate control from myopic ex-vivo fixed chicken retinas. Our results provide a baseline analysis of differences in retinal cell packing density between both types of eyes. Since no staining is necessary the sample receives less treatment and the observed histological features may reflect the natural morphology in a better way. The potential combination of this technology with electrophysiological recordings with microelectrode arrays might provide additional information on the details of myopia development and emmetropization.

### **Acknowledgments**

This work has been supported by “Ministerio de Ciencia e Innovación”, Spain (grants FIS2010-14926 and CSD2007-00013 SAUUL); Fundación Séneca (Region de Murcia, Spain), grant 4524/GERM/06 and EU FEDER funds. The authors would like to thank Eva Burkhardt from the Institute for Ophthalmic Research (Tuebingen, Germany) for helping in the preparation of retinal tissues.